




Article

Development and Evaluation of *Elaeagnus rhamnoides* (L.) A. Nelson Oil-Loaded Nanostructured Lipid Carrier for Improved Skin Hydration

Chaiyavat Chaiyasut ¹, Bhagavathi Sundaram Sivamaruthi ^{2,*}, Patchareepon Jungsinyatam ¹,
Chawin Tansrisook ¹, Damrongsak Jinarat ^{1,3}, Khontaros Chaiyasut ⁴, Sartjin Peerajan ⁵
and Wandee Rungseevijitprapa ^{3,6,*}

¹ Innovation Center for Holistic Health, Nutraceuticals, and Cosmeceuticals, Faculty of Pharmacy, Chiang Mai University, Chiang Mai 50200, Thailand

² Office of Research Administration, Chiang Mai University, Chiang Mai 50200, Thailand

³ Department of Pharmaceutical Chemistry and Technology, Faculty of Pharmaceutical Sciences, Ubon Ratchathani University, Ubon Ratchathani 34190, Thailand

⁴ Institute of Research and Development, Chiang Mai Rajabhat University, Chiang Mai 50300, Thailand

⁵ Health Innovation Institute, Chiang Mai 50200, Thailand

⁶ School of Cosmetic Science, Mae Fah Luang University, Muang District, Chiang Rai 57100, Thailand

* Correspondence: sivamaruthi.b@cmu.ac.th (B.S.S.); wandee.run@mfu.ac.th (W.R.)

Featured Application: The study describes the optimum conditions to produce a sea buckthorn oil-loaded nanostructured lipid carrier (SBO-NLC) for improved skin hydration. The results suggested that the SBO-NLC could be a potent agent for preventing skin dehydration.



Citation: Chaiyasut, C.; Sivamaruthi, B.S.; Jungsinyatam, P.; Tansrisook, C.; Jinarat, D.; Chaiyasut, K.; Peerajan, S.; Rungseevijitprapa, W. Development and Evaluation of *Elaeagnus rhamnoides* (L.) A. Nelson Oil-Loaded Nanostructured Lipid Carrier for Improved Skin Hydration. *Appl. Sci.* **2022**, *12*, 8324. <https://doi.org/10.3390/app12168324>

Academic Editor: Jongsung Lee

Received: 1 July 2022

Accepted: 16 August 2022

Published: 20 August 2022

Publisher's Note: MDPI stays neutral with regard to jurisdictional claims in published maps and institutional affiliations.



Copyright: © 2022 by the authors. Licensee MDPI, Basel, Switzerland. This article is an open access article distributed under the terms and conditions of the Creative Commons Attribution (CC BY) license (<https://creativecommons.org/licenses/by/4.0/>).

Abstract: Sea buckthorn (SB) (*Elaeagnus rhamnoides* (L.) A. Nelson) is rich in flavonoids, phenolic compounds, anthocyanins, carotenoids, and phytosterol. Its phytochemicals exhibit various biological activities, such as antioxidant, immunomodulatory and anti-carcinogenic activities. SB also helps prevent the development of wrinkles and protects the skin's surface from UV rays. The purpose of the present study was to develop and characterize an SB oil (SBO)-loaded nanostructured lipid carrier (NLC) for improved skin hydration. The response surface methodology (RSM) and central composite design (CCD) were employed to optimize the influencing factors (wax percentage, surfactant percentage, and PEG400 percentage in the surfactant) to achieve the desirable qualities in SBO-NLCs. The optimum (minimum) size of SBO-NLCs (105.26 nm) was obtained with a combination of 2.5% wax, 7.5% surfactant, and 30% PEG400 in the surfactant. A narrow polydispersity index (PDI; 0.16), relatively low zeta potential (ZP; -15.63 mV), and high entrapment efficiency (EE; 90.88%) were observed in this study. Reduced quadratic and reduced 2FI models were adapted to predict conditions to attain the optimum size and PDI of SBO-NLCs, respectively. ZP and EE were predicted with the help of a reduced cubic model. All of the predicted models were statistically significant. Differential scanning calorimetry results suggested that the SBO-NLCs had less crystallinity and therefore reduced the rate of drug expulsion from the inner core of the NLCs. A noticeable level of occlusion effect was observed in the SBO-NLCs. The SBO-NLCs showed a faster vitamin E (biomarker for the drug) release rate into the skin within 24 h, and the released vitamin E level after 48 h was significantly higher than that for the free SBO. Additionally, SBO-NLCs delivered vitamin E into the inner skin significantly (22.73 ± 1.67 $\mu\text{g}/\text{cm}^2$ of skin). In conclusion, the SBO-NLC is a potential delivery system that can be used to prevent skin water loss and improve skin hydration. Further investigations, such as drug stability and safety evaluations, are required prior to commercialization for human use.

Keywords: sea buckthorn; *Elaeagnus rhamnoides* (L.) A. Nelson; nanostructured lipid carrier; skin hydration; response surface methodology; central composite design

1. Introduction

Skin is a complex and the largest organ (accounting for roughly 16%) of the body, involved in protection against physical, chemical, and microbial violence, vitamin synthesis, temperature regulation, and maintaining the body's moisture content. The outermost layer of skin, the stratum corneum (SC), contains ~10–20% water and is filled with corneocytes to delay water loss. The loss of skin moisture affects the functions of the skin, and the use of moisturizer aids in restoring the functionality of the skin and improves skin health [1–3].

Moisturizers with bioactive compounds provide moisture to the skin and can be used to treat dermatological diseases [4]. They must preserve the optimal balance between water and skin lipids by maintaining the water content in the skin. A typical moisturizer may contain humectants (hygroscopic substances that improve the water-retaining ability of the SC), emollients or occlusive agents (to prevent the evaporation of water from the SC), and lipids [5].

Cosmetic formulations, especially skincare products with nano-structured lipid carriers (NLCs), are superior moisturizing agents, improving the skin permeation and stability of active compounds. NLCs are lipid nanoparticles suitable for application to the skin. Mixtures of solid lipids and liquid lipids (in ratios of 70:30 to 99.9:0.1) are constitutive of NLCs [5]. Topical formulations with occlusive properties are used to keep the skin adequately hydrated and the SC intact. Customers prefer emulsions with sufficient occlusive and cosmetically acceptable properties. NLCs are preferred due to their ability to stabilize active compounds, their bioavailability, precise occlusion, film formation, skin hydration properties, etc. [6]. Cutanova Nanorepair Q10 cream, an NLC-containing cosmetic product marketed in 2005, provides high skin hydration, a better consistency, and better spreadability on the skin compared to a water-in-oil cream [7].

Sea buckthorn (SB) (*Elaeagnus rhamnoides* (L.) A. Nelson), previously called *Hippophae rhamnoides* L., belongs to *Hippophae* L. and is cultivated primarily in China and Russia [8,9]. SB is traditionally used for food and medicine in Asia and Europe. SB is rich in flavonoids, phenolic compounds, anthocyanins, carotenoids, and phytosterol, and its extracts and oil are known for antimicrobial, anti-inflammatory, antioxidant, anti-cancer, hepatoprotective, neuroprotective, antifatigue, and cardioprotective activities [9–12]. SB was also reported to have skin protection and health properties. SB oil (SBO) improved atopic dermatitis-like skin lesions by inhibiting the activation of chemokines in the skin [13]. SBO could minimize UV-induced skin damage and skin aging [14,15].

The bioactivities of SBO attract the developer and cosmetician for use in their formulations. The development of NLC-based skincare products with SBO could increase skin hydration and prevent photo-damage to the skin. To this end, the present study was undertaken to develop, optimize, and characterize an SBO-loaded NLC (SBO-NLC) for skin hydration.

The response surface methodology (RSM) and central composite design (CCD) have been employed to reduce experimental burdens and optimize the several influencing factors in extraction conditions, fermentation processes, and other optimization studies [16–18]. Thus, we adapted the RSM and CCD for the experimental design and the optimization of the selected variable factors.

2. Materials and Methods

2.1. Materials

SBO was obtained from Jiangxi Yisenyuan Plant Spices Co., Ltd., Ji'an, Jiangxi, China. Glyceryl monostearate, poloxamer 407, and polyethylene glycol 400 were purchased from Sigma-Aldrich Inc., St. Louis, MO, USA. Tween 80 was obtained from Acros Organics, Morris Plains, NJ, USA. Acetonitrile, methanol, and other analytical chemicals were purchased from RCI Labscan Ltd., Bangkok, Thailand.

2.2. Preparation of Blank NLCs

The blank NLCs were prepared by the melt emulsification method, as detailed previously [19], with some modifications. Briefly, the following ingredients were blended using a homogenizer (Ultra-turrax T10, IKA, Königswinter, Germany) for 5 min at 12,000 rpm. The solid lipid (Glyceryl monostearate) and liquid lipid SBOs were maintained at 70–75 °C. The aqueous phase consisted of the surfactant (1:1 ratio of tween 80: poloxamer 407), co-surfactant (polyethylene glycol 400; PEG400), and water heated to 75–80 °C. Then, the hot pre-emulsion was subjected to the probe-type ultrasonication process (80% amplitude for 4 min; Vibracell VC50T, Sonics & Materials Inc., Newtown, CT, USA) to reduce the particle size, and the process was repeated twice (with a resting time of 1 min for each cycle). The particles were allowed to cool at room temperature to obtain the blank NLCs.

2.3. Development of SBO-Loaded NLCs (SBO-NLCs)

Three independent variables, such as the amount of solid lipid, the concentration of surfactant, and the percentage of PEG400 in the surfactant influenced the NLC properties. A fixed concentration of SBO (5%) was used in the SBO-NLC preparation. Three levels of each variable were studied to determine each variable's optimum level and obtain the optimum NLC formulation for topical use [20]. The response surface methodology (RSM) and central composite design (CCD) were employed using Design expert version 10 (Stat-Ease Inc., Minneapolis, USA). The experiment design is shown in Table 1. The various concentrations of solid lipids (2.5–7.5% *w/w*; X_1), surfactant (Tween 80 and poloxamer 407 at 1:1 ratio; 2.5–7.5% *w/w*; X_2), and co-surfactant (PEG 400; 10–30% *w/w*; X_3) were used to prepare the optimum SBO-NLCs. The particle size (Y_1), polydispersity index (Y_2), zeta potential (Y_3), and entrapment efficiency (Y_4) of the SBO-NLCs were studied (Formula (1)).

$$Y = b_0 + b_1X_1 + b_2X_2 + b_3X_3 + b_{12}X_1X_2 + b_{13}X_1X_3 + b_{23}X_2X_3 + b_{11}X_1^2 + b_{22}X_2^2 + b_{33}X_3^2 \quad (1)$$

where Y is the response of the dependent factor; b_0 is a constant; b_1 , b_2 , and b_3 represent the slope efficiency of the linear equation; b_{12} , b_{13} , and b_{23} represent the efficiency between control variables; and b_{11} , b_{22} , and b_{33} represent the quadratic efficiency yielded by the experiment.

Table 1. The variable factors and their concentrations for the preparation of the NLCs.

STD	Wax (%)	Surfactant (%)	PEG400 in Surfactant (%)
1	2.50	2.50	10.00
2	7.50	2.50	10.00
3	2.50	7.50	10.00
4	7.50	7.50	10.00
5	2.50	2.50	30.00
6	7.50	2.50	30.00
7	2.50	7.50	30.00
8	7.50	7.50	30.00
9	0.79	5.00	20.00
10	9.20	5.00	20.00
11	5.00	0.79	20.00
12	5.00	9.20	20.00
13	5.00	5.00	3.18
14	5.00	5.00	36.81
15	5.00	5.00	20.00
16	5.00	5.00	20.00
17	5.00	5.00	20.00

2.4. Particle Size, Polydispersity Index (PDI), and Zeta Potential (ZP)

The sample dispersions were diluted with deionized water at a ratio of 1:40. The average particle size (Z average), PDI, and ZP of the SBO-NLCs were measured using photon

correlation spectroscopy (Zetasizer[®] Nano ZS90, Malvern Panalytical, Great Malvern, UK), as detailed previously [21]. The measurements were performed in triplicate at 25 °C.

2.5. Entrapment Efficiency (EE)

The total amount of vitamin E (vitamin E was used as the standard biomarker for the drug) in the SBO-NLCs was determined by centrifugal filtration [22]. Briefly, 100 µL of the sample was filtered by a centrifugal filter (0.5 mL, 15 kDa; Amicon[®] Ultra, Merck Ltd., Darmstadt, Germany) at 8000 rpm and 4 °C for 10 min. Then, the particles were washed with 100 µL deionized water and centrifuged at 8000 rpm for 10 min. The particles were kept in 400 µL deionized water using reverse spin. Then, the particles were dissolved in methanol using an ultrasonic bath for 15 min. The solution was filtered and analyzed using the HPLC system (C18 column; 150 mm × 3.9 mm × 5 µm; Dionex/Thermo Ultimate 3000 (Thermo Fisher, Waltham, MA, USA). The mobile phase consisted of acetonitrile and deionized water. The flow rate was 1.0 mL/min, and the column temperature was controlled at 45 °C. UV detection was performed at 294 nm.

The percentage of EE was calculated according to Equation (2):

$$EE \% = \frac{w_{entrapped}}{w_{initial}} \times 100 \quad (2)$$

where $W_{entrapped}$ is the amount of drug entrapped in the SBO-NLCs and $W_{initial}$ is the amount of the total SBO used for the NLC preparation.

2.6. Differential Scanning Calorimetry (DSC)

The thermal transformations of the SBO-NLCs and the blank NLCs were evaluated using DSC (DSC 822e, Mettler Toledo, Greifensee, Switzerland), as described previously [23]. Briefly, 1.5 mL of SBO-NLCs and the blank NLCs were kept at −20 °C for 24 h and then freeze-dried. The dried samples (~3.0 mg) were placed in an aluminum pan and heated from 25 to 80 °C at a rate of 10 °C/min, under nitrogen gas, at a flow rate of 30 mL/min.

2.7. Microscopy Analysis

The morphology and size of the SBO-NLCs were determined using transmission electron microscopy (TEM) (JEM-2011, JEOL, Tokyo, Japan) [24]. A single drop of SBO-NLCs was positioned onto a copper grid and stained with 1% phosphotungstic acid, and the grid was dried at room temperature before analysis. The TEM analysis was achieved at 100 kV. A representative SBO-NLC sample was analyzed to confirm morphology and size.

2.8. In Vitro Occlusion Effect

The in vitro occlusion property of SBO-NLCs was studied as detailed by Krambeck et al. [25], with slight modifications. Briefly, 350 mg of the sample or petroleum jelly (Vaseline brand; positive control) was spread on the filter paper (Whatman No. 1) and placed over a beaker containing 25 mL of deionized water. The empty filter paper was used as a negative control. Then, the beakers were incubated at 32 °C with a controlled relative humidity of 50–55%. The weight of the beaker containing water was determined at the initial conditions and after 6, 12, 24, 48, and 72 h.

2.9. In Vitro Drug Release Studies

The dialysis bag technique was used to study the in vitro drug release property of the SBO-NLCs [26]. The samples (1.0 mL) were placed into a dialysis bag (molecular weight cut-off: 12,400; Sigma-Aldrich Inc., St. Louis, MO, USA). Both ends of the bag were tightened and sealed, then placed in a buffer-filled bottle (20% ethanol in PBS, pH 5.5, 200 mL). The buffer samples were collected at predetermined intervals (1, 3, 6, 12, 24, and 48 h) and the vitamin E content, the standard marker for the drug, was determined.

2.10. Determination of the In Vitro Skin Permeation of SBO-NLCs

The permeation study was carried out using pig ear skin, as detailed previously [21]. The pig ear was purchased from the local market, Chiang Mai, and processed to remove the fat layer. The processed skin was used as the membrane for the Franz diffusion cell. An amount of 500 μ L of SBO-NLCs was placed in the donor chamber, and PBS (pH 7.4) served as the medium. After 12 and 24 h, 300 μ L of the sample (from the receiver chamber) was collected for analysis. After 24 h, twenty pig skin tape strips were removed. Vitamin E was extracted from tape strips using methanol in an ultrasonic bath for 15 min. The retained skin was cut into small pieces with scissors and extracted using methanol in an ultrasonic bath for 15 min. The methanol solution was analyzed for vitamin E in the skin by HPLC to determine the release of SBO.

2.11. Statistical Analysis

All data are shown as means \pm standard deviations (SDs). The means of two data sets were statistically compared using the Student's *t*-test. The means of more than two data sets were statistically compared using two-way ANOVA and Tukey's multiple comparison test. RSM data analysis was performed using the Design-Expert Program version 10.0 (Stat-Ease Inc., Minneapolis, MN, USA) and ANOVA to define the significance of variable factors used in the study.

3. Results

3.1. Development of SBO-NLCs

A total of seventeen experiments, including three center point standard (STD) runs (5% wax, 5% surfactant, 20% PEG400 in the surfactant; STDs 15, 16, 17), were predicted and performed to develop the optimum SBO-NLCs.

3.2. Size of SBO-NLCs

The predicted size of center point STDs was 184.62 nm, whereas the actual SBO-NLC sizes varied (198.43, 167.23, and 163.10 nm). The optimum-sized SBO-NLCs (i.e., the smallest size: 105.26 nm) were generated with a combination of 2.5% wax, 7.5% surfactant, and 30% PEG400 in the surfactant (Table 2).

Table 2. The predicted and observed values for size, polydispersity index, zeta potential, and entrapment efficiency. * Excluded from the analysis.

STD	Size		Polydispersity Index		Zeta Potential		Entrapment Efficiency	
	Actual	Predicted	Actual	Predicted	Actual	Predicted	Actual	Predicted
1	144.40	156.09	0.16	0.18	−27.88	−29.77	51.07	50.74
2	214.57	225.22	0.26	0.26	−26.03	−28.85	89.21	88.63
3	134.25	138.61	0.37	0.37	−30.67	−33.31	69.68	69.59
4	158.13	178.25	0.33	0.34	−34.03	−35.98	38.25	38.21
5	156.13	160.60	0.14 *	0.25	−17.73	−19.46	85.25	84.69
6	226.37	229.73	0.32	0.33	−17.75	−18.55	30.42	30.22
7	105.27	119.20	0.26	0.27	−20.60	−21.45	84.56	84.45
8	162.80	158.84	0.25	0.24	−22.57	−24.12	50.47	50.41
9	112.53	99.84	0.29	0.26	−16.33	−17.07	52.31	52.61
10	201.47	191.31	0.32	0.30	−36.33	−37.07	58.93	59.27
11	235.57	221.78	0.23	0.24	−24.03	−21.45	55.00	55.66
12	163.80	147.47	0.31	0.32	−31.57	−29.12	55.30	55.27
13	217.90	190.89	0.33	0.29	−36.87	−36.39	78.63	79.07
14	188.10	178.35	0.30	0.27	−15.63	−17.75	57.08	57.40
15	198.43	184.62	0.27	0.28	−33.80	−27.07	90.88	82.76
16	167.23	184.62	0.26 *	0.28	−33.06 *	−27.07	76.75	82.76
17	163.10	184.62	0.26	0.28	−32.63	−27.07	81.42	82.76

The reduced quadratic model was adapted for the SBO-NLC size analysis. The model was significant ($p = 0.0010$), and the lack-of-fit value was non-significant ($p = 0.6268$). Acceptable ranges of adjusted R^2 (0.7681) and predicted R^2 (0.5924) values were detected in the reduced quadratic model (Table 3).

Table 3. Analysis of variance for the size, polydispersity index (PDI), zeta potential (ZP), and entrapment efficiency (EE).

Responses	Models	Model (p-Value)	Lack of Fit (p-Value)	R ²	Adjusted R ²	Predicted R ²	Adequate Precision
Size	Reduced quadratic	0.0010	0.6268	0.8551	0.7681	0.5924	10.9504
PDI	Reduced 2FI	0.0017	0.1280	0.8487	0.7646	0.5934	12.0536
ZP	Reduced cubic	0.0085	0.1503	0.8505	0.7196	0.5654	7.1890
EE	Reduced cubic	0.0019	0.9703	0.9902	0.9609	0.9587	19.9901

The values suggested that the reduced quadratic model was appropriate for predicting SBO-NLC size. The CCD-generated reduced quadratic equation for SBO-NLC size was as follows (Formula (3)):

$$\text{Size} = 73.2372 + 38.8639A + 1.8463B + 0.8235C - 1.1797AB - 0.2393BC - 2.2088A^2 \quad (3)$$

where A = the percentage of wax in the formulation (2.5 to 7.5%), B = the percentage of surfactant in the formulation (2.5 to 7.5%), and C = the percentage of PEG400 in the surfactant (10 to 30%).

The concentrations of wax and surfactant greatly influence the size of NLCs. The minimum concentration of wax and a high concentration of surfactant yielded smaller NLCs. The percentage (%) of PEG in the surfactant was not an influencing factor with respect to the size of NLCs (Figure 1).

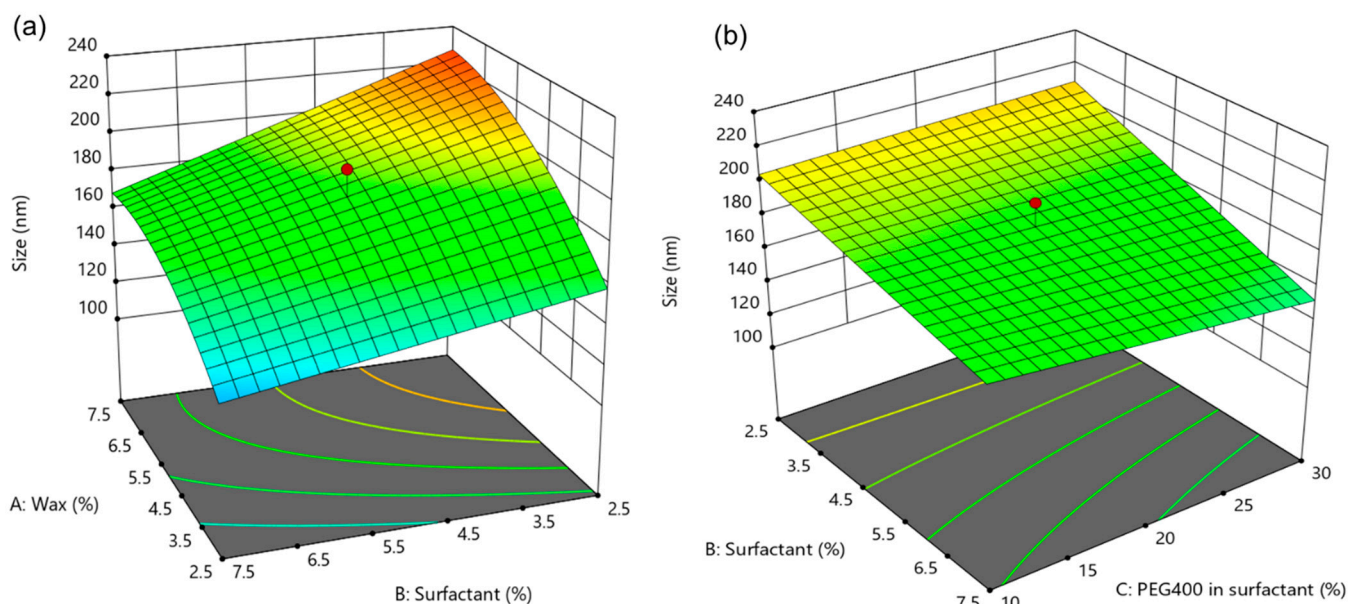


Figure 1. The response surface plot presents the effects of wax, surfactant, and percentage of PEG in the surfactant on the size of SBO-NLCs. (a) Interaction of wax and surfactant. (b) Interaction of surfactant and percentage of PEG400 in the surfactant.

3.3. Polydispersity Index (PDI) of the SBO-NLCs

The predicted and actual PDI value of center point STDs was 0.26. A low PDI value of 0.16 was observed in the combination of 2.5% wax, 2.5% surfactant, and 10% PEG400 in the

surfactant (Table 2). The reduced 2FI model was adapted for the PDI of SBO-NLCs. The model was significant ($p = 0.0017$), and the lack-of-fit value was non-significant ($p = 0.1280$). Acceptable ranges of adjusted R^2 (0.7646) and predicted R^2 (0.5934) values were detected in the reduced 2FI model (Table 3). The results recommended that the reduced 2FI model was appropriate for predicting the PDI of SBO-NLCs. The CCD-generated reduced 2FI model equation for the PDI of SBO-NLCs was as follows (Formula (4)):

$$\text{PDI} = -0.0644 + 0.0269A + 0.0669B + 0.0081C - 0.0043AB - 0.0018BC \quad (4)$$

where A = the percentage of wax in the formulation (2.5 to 7.5%), B = the percentage of surfactant in the formulation (2.5 to 7.5%), and C = the percentage of PEG400 in the surfactant (10 to 30%).

The concentrations of surfactant, wax, and PEG400 in the surfactant were the influencing factors on the PDI of the NLCs. Lower concentrations of surfactant and wax and a lower percentage of PEG in the surfactant produced SBO-NLCs with lower PDI values. The influences of variable factors on the PDI of the NLCs are represented in Figure 2.

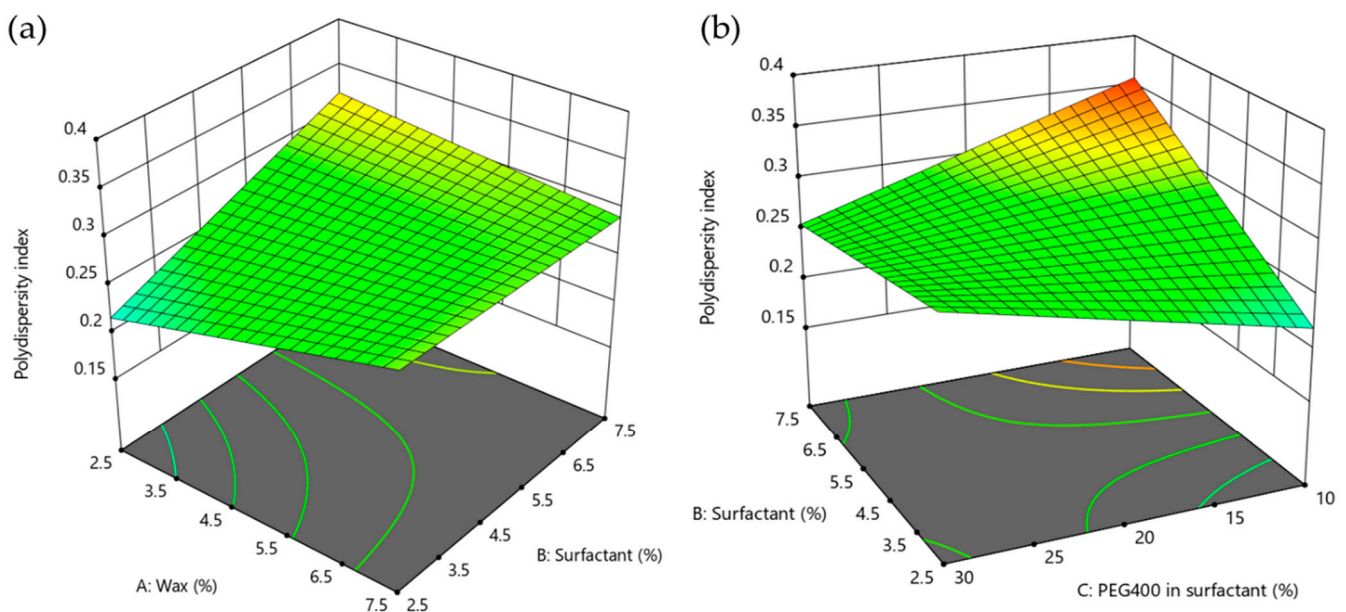


Figure 2. The response surface plot presents the effects of wax, surfactant, and PEG in the surfactant on the polydispersity index of SBO-NLCs. (a) Interaction of wax and surfactant. (b) Interaction of surfactant and PEG400 percentage in the surfactant.

3.4. Zeta Potential (ZP) of SBO-NLCs

SBO-NLCs with the optimum ZP were predicted (-17.07 mV) in STD run 9, whereas the actual optimum ZP (-15.63 mV) was observed in STD 14. The predicted ZP value of the center point STDs was -27.07 mV, but the actual values were different (Table 2). The reduced cubic model was employed for the prediction of the ZP of the SBO-NLCs. The model was significant ($p = 0.0085$) and the lack-of-fit value was non-significant ($p = 0.1503$). Acceptable ranges of adjusted R^2 (0.7196) and predicted R^2 (0.5654) values were detected in the reduced cubic model (Table 3). The results recommended that the reduced cubic model was appropriate for predicting the ZP of SBO-NLCs.

The CCD-generated reduced cubic model equation for the ZP of SBO-NLCs was as follows (Formula (5)):

$$\text{ZP} = -65.2627 + 7.1499A + 16.1094B + 0.4764C - 3.6681AB + 0.0155BC - 1.6616B^2 + 0.3525AB^2 \quad (5)$$

where A = the percentage of wax in the formulation (2.5 to 7.5%), B = the percentage of surfactant in the formulation (2.5 to 7.5%), and C = the percentage of PEG400 in the surfactant (10 to 30%).

The concentration of wax and the percentage of PEG400 in the surfactant significantly influenced the ZP of the SBO-NLCs. The high content of wax and low percentage of PEG400 in the surfactant generated SBO-NLCs with a lower ZP. The surfactant concentration did not significantly affect the ZP of the SBO-NLCs (Figure 3).

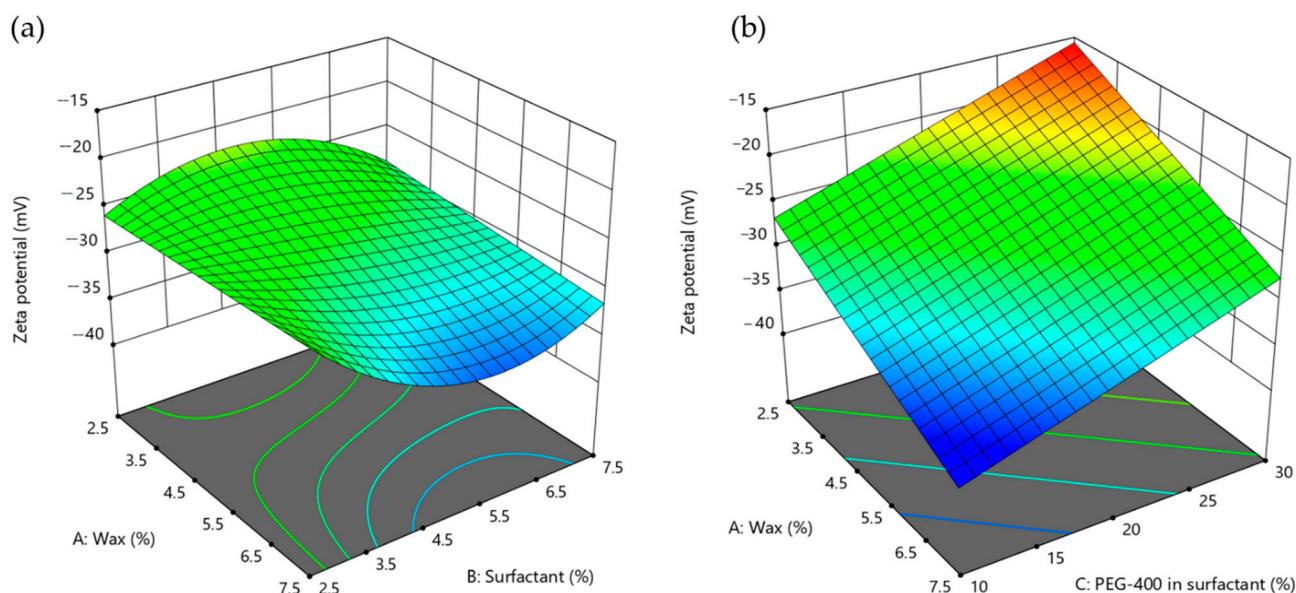


Figure 3. The response surface plot presents the effects of wax, surfactant, and PEG percentage in the surfactant on the zeta potential of the SBO-NLCs. (a) Interaction of wax and surfactant. (b) Interaction of wax and PEG400 percentage in the surfactant.

3.5. Entrapment Efficiency (EE) of the SBO-NLCs

The predicted EE value of the SBO-NLCs for center point STDs was 82.76%, whereas the actual EE of SBO-NLCs was varied (90.88, 76.75 and 81.42%). The highest EE (90.88%) was observed in one of the center points runs (STD 15; 5% Wax, 5% Surfactant, 20% PEG400 in the surfactant). The actual lowest EE (30.42%) was found in STD 6 (Table 2). The reduced cubic model was adapted for the prediction of EE of the SBO-NLCs. The model was significant ($p = 0.0019$) and the lack-of-fit value was non-significant ($p = 0.9703$). Acceptable ranges of adjusted R^2 (0.9609) and predicted R^2 (0.9587) values were detected in the reduced cubic model (Table 3). The results recommended that the reduced cubic model was appropriate for predicting the EE of SBO-NLCs.

The CCD-generated reduced cubic model equation for the EE of the SBO-NLCs was as follows (Formula (6)):

$$\%EE = 10^{0.9123+0.2949A-0.0990B+0.0644C+0.0304AB-0.0163AC-0.0050BC-0.0213A^2+0.0227B^2-0.0003C^2+0.0015ABC+0.0006A^2C-0.0065AB^2} \quad (6)$$

where A = Percentage of wax in formulation (2.5 to 7.5%), B = Percentage of surfactant in formulation (2.5 to 7.5%), C = Percentage of PEG400 in the surfactant (10 to 30%).

All the studied variable factors substantially affected the EE of the SBO-NLCs. The higher content of wax, surfactant and PEG400 percentage in the surfactant increased the EE of the SBO-NLCs (Figure 4).

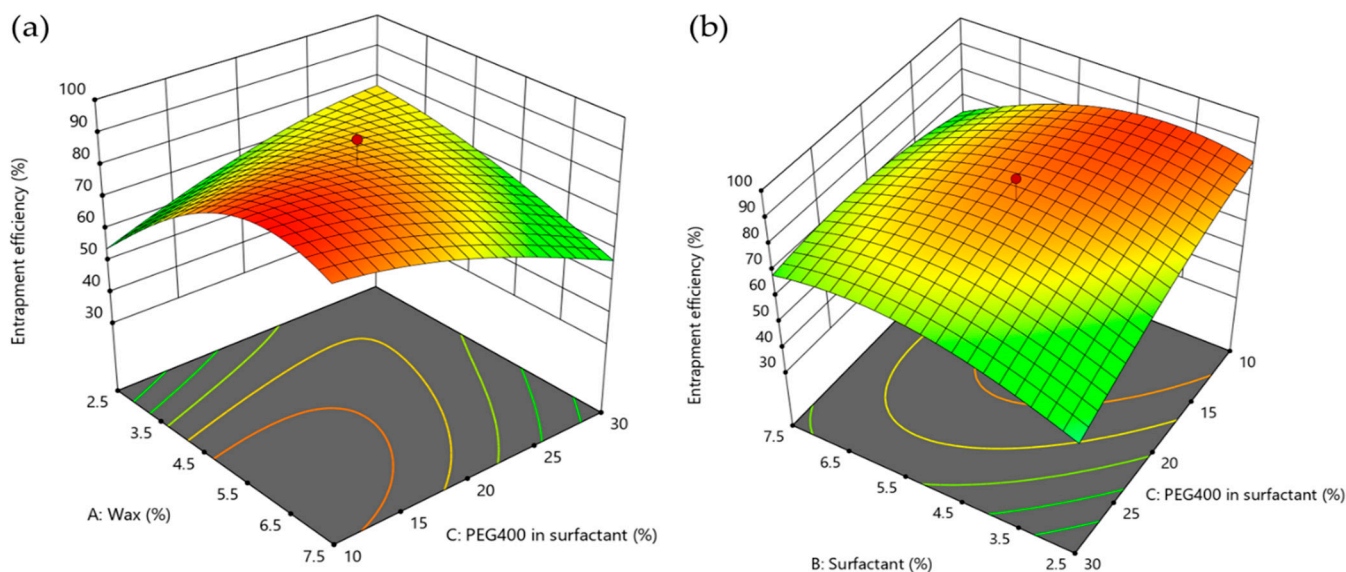


Figure 4. The response surface plot presents the effects of wax, surfactant, and PEG percentage in the surfactant on the entrapment efficiency of the SBO-NLCs. (a) Interaction of wax and PEG400 percentage in the surfactant. (b) Interaction of surfactant and PEG400 percentage in the surfactant.

The wax (%) ($p = 0.003$) and surfactant concentration (%) ($p = 0.013$) and %wax² ($p = 0.0225$) significantly influenced the particle size of the SBO-NLCs.

Surfactant concentration (%; $p = 0.0083$), wax × surfactant concentration (%; $p = 0.240$), and %surfactant × %PEG400 in surfactant ($p = 0.0017$) significantly manipulated the PDI of the SBO-NLCs.

Wax concentration (%; $p = 0.0070$), %PEG400 in surfactant ($p = 0.0008$), and %wax × %surfactant² ($p = 0.0343$) substantially affected the ZP of the SBO-NLCs.

The EE of the SBO-NLCs was influenced by the percentage of PEG400 in the surfactant ($p = 0.0212$), %wax × %surfactant ($p = 0.0210$), %wax × %PEG400 in surfactant ($p = 0.0010$), %surfactant × %PEG400 in surfactant ($p = 0.0040$), %wax² ($p = 0.0016$), %surfactant² ($p = 0.0015$), %PEG400 in surfactant² ($p = 0.0166$), %wax × %surfactant × %PEG400 in surfactant ($p = 0.0007$), and %wax² × %PEG400 in surfactant ($p = 0.0023$) (Table 4).

Table 4. The estimated variables for the SBO-NLC preparation and its properties.

Terms	Estimated Parameters							
	Size	<i>p</i> -Value	PDI	<i>p</i> -Value	ZP	<i>p</i> -Value	EE *	<i>p</i> -Value
%Wax (A)	27.1940	0.0003	0.0131	0.1083	−5.9460	0.0070	0.0154	0.2426
%Surfactant (B)	−22.0925	0.0013	0.0246	0.0083	−2.2804	0.0646	−0.0009	0.9063
%PEG400 in Surfactant (C)	−3.7271	0.4733	−0.0071	0.3566	5.5408	0.0008	−0.0414	0.0212
%Wax × %Surfactant (A × B)	−7.3729	0.2856	−0.0271	0.0240	−0.8950	0.5380	−0.0349	0.0210
%Wax × %PEG400 (A × C)							−0.0817	0.0010
%Surfactant × %PEG400 (B × C)	−5.9812	0.3816	−0.0441	0.0017	0.3883	0.7872	0.0561	0.0040
%Wax × %Wax (A ²)	−13.8050	0.0225					−0.0604	0.0016
%Surfactant × %Surfactant (B ²)					0.6302	0.5890	−0.0615	0.0015
%PEG400 × %PEG400 (C ²)							−0.0316	0.0166
%Wax × %Surfactant × %PEG400 (ABC)							0.0908	0.0007
%Wax × %Surfactant × %Surfactant (A × B ²)					5.5077	0.0343	−0.1016	0.0023
%Wax × %Wax × %PEG400 (A ² × C)							0.0363	0.0688

PDI: Polydispersity index; ZP: Zeta potential; EE: Entrapment efficiency. * Logarithm transformation was implemented to assess the EE.

3.6. Differential Scanning Calorimetry Analysis

The endothermic DSC thermograms showed that the melting points of the glyceryl monostearate (solid lipid), poloxamer 407, SBO-NLCs, and blank NLCs were 73.79, 54.45,

65.72, and 44.09 °C, respectively (Figure 5). The crystalline nature of the bulk solid lipid, represented as enthalpy, was reduced from -167.05 J/g to -26.45 and -27.69 J/g of the solid matrix in the blank NLCs and SBO-NLCs, respectively (Figure 5, Table 5).

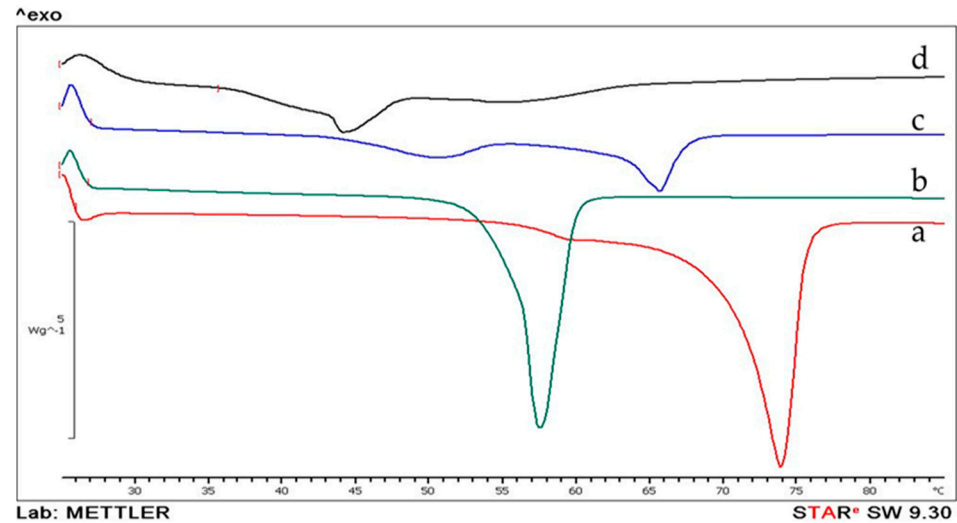


Figure 5. Differential scanning calorimetry thermograms of glyceryl monostearate (a), poloxamer 407 (b), SBO-NLCs (c), and blank NLCs (d).

Table 5. The melting and enthalpy profile of the SBO-NLC and its composition.

Samples	Melting Point (°C)	Enthalpy (J/g)
Glyceryl monostearate	73.79	-167.05
Poloxamer407	57.45	-105.38
Blank NLC	44.09	-26.45
SBO-NLC	65.72	-27.69

3.7. TEM Analysis

The TEM analysis showed that the prepared SBO-NLC samples were in the predicted and observed size range (~ 140 – 200 nm) and that they had a spherical shape (Figure 6).

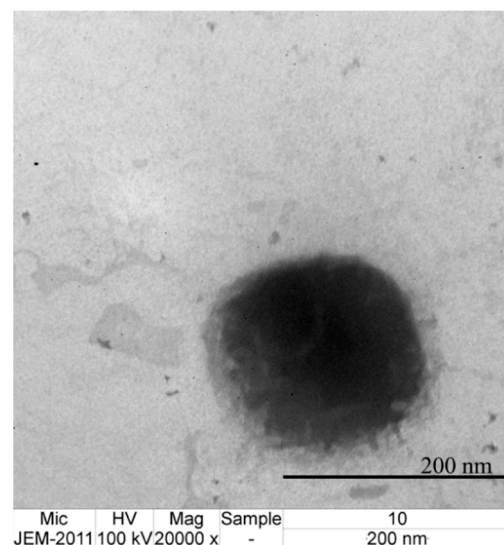


Figure 6. Transmission electron microscopic image of a representative SBO-NLC.

3.8. In Vitro Occlusion Effect of the SBO-NLCs

The occlusion effect of the SBO-NLCs in terms of water loss (%) according to specified time is represented in Figure 7. After 72 h of incubation, 1.85 ± 0.17 , 0.86 ± 0.17 , and $3.74 \pm 0.26\%$ water loss was observed in the SBO-NLCs, petroleum jelly, and DI water, respectively.

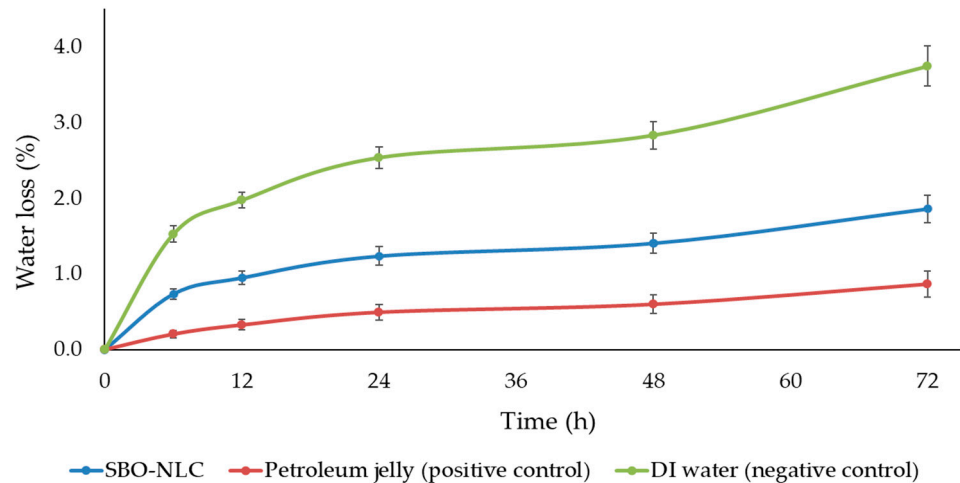


Figure 7. Graphical representation of occlusion effect (percentage water loss) of the SBO-NLCs. Petroleum jelly served as the positive control.

3.9. In Vitro Release

The in vitro release profile of vitamin E is presented in Figure 8. A constant vitamin E release profile was observed during the initial period. During the first 24 h, the rate of vitamin E release from the SBO-NLC samples was slightly faster compared to the free SBO. Following 24 h, the vitamin E release rate from the free SBO remained constant, whereas significant vitamin E release was observed in the SBO-NLCs. In detail, the cumulative vitamin E release of the SBO-NLCs was higher than that of the free SBO. The cumulative release of vitamin E from the SBO-NLCs was 9.2 ± 0.20 and $17.8 \pm 0.50\%$ after 24 and 48 h, respectively, whereas the release of vitamin E from the free SBO was 7.3 ± 0.97 and $8.4 \pm 1.68\%$ after 24 and 48 h, respectively (Figure 8).

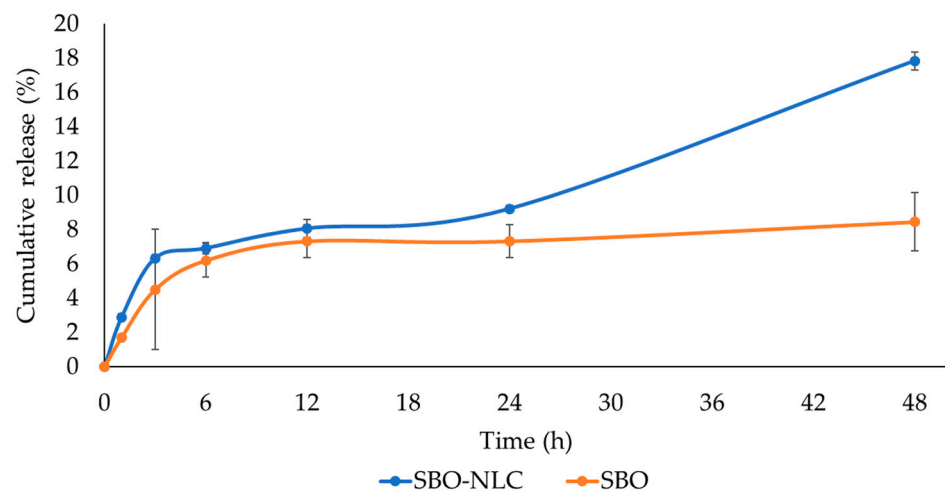


Figure 8. Graphical representation of the cumulative release profile of the SBO-NLCs. Significantly different from the free SBO.

3.10. In Vitro Skin Permeation of the SBO-NLCs

The in vitro skin permeation of the SBO-NLCs and the SBO was studied using Franz-type diffusion cells. A higher cumulative vitamin E (the biomarker for the drug) permeation level was observed in the free SBO-treated samples ($6.74 \pm 0.83\%$) than in the SBO-NLC-treated samples ($3.44 \pm 0.85\%$) ($p < 0.05$) (Figure 9). The amount of vitamin E was higher in the inner skin and skin tape of the SBO-NLC-treated samples (22.73 ± 1.67 and $3.75 \pm 0.60 \mu\text{g}/\text{cm}^2$, respectively) than in the free SBO-treated samples (2.13 ± 0.04 and $0.27 \pm 0.00 \mu\text{g}/\text{cm}^2$, respectively) (Figure 9). Vitamin E permeation was significantly ($p < 0.05$) higher in the inner skin of the pig ear skin, which suggested that the prepared NLCs could deliver the drug appropriately.

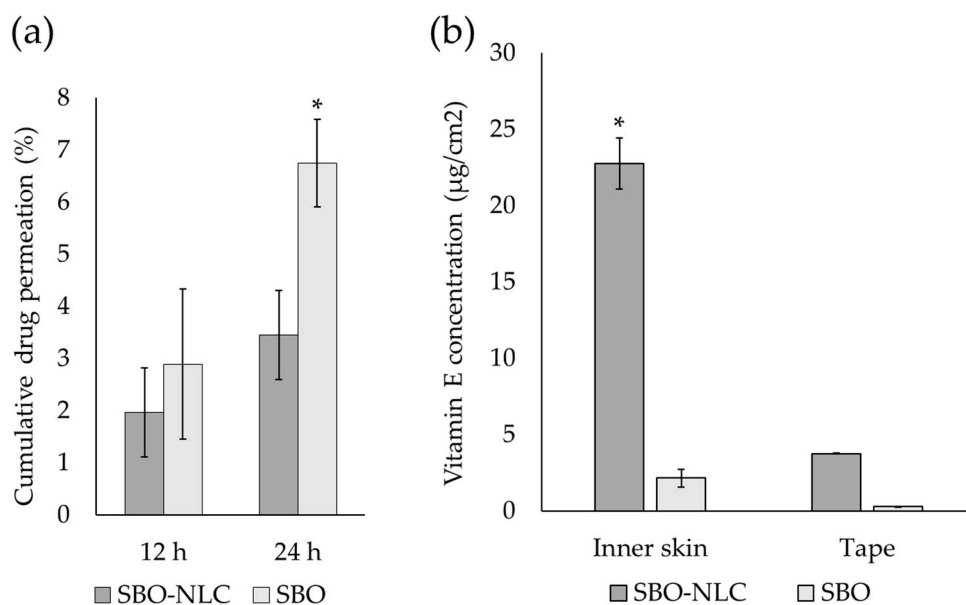


Figure 9. The in vitro drug permeation property of the SBO-NLCs. (a) The cumulative vitamin E permeation level (%) at 12 and 24 h. * A significant level of free SBO penetration was observed after 24 h. (b) The penetration of SBO, represented in terms of vitamin E concentration, into the inner skin. * A significant level of vitamin E penetrated the inner skin compared to the free SBO.

4. Discussion

SBO and SB extracts have been recognized as ingredients for use in skincare products for the treatment of chronic inflammatory conditions, such as psoriasis and atopic dermatitis (AD). SB fruit pulp oil (SBFO) is rich in mono- and polyunsaturated and saturated fatty acids. This lipopolysaccharide-induced expression of nuclear factor-kappa-b (NF- κ b) and release of free radicals, pro-inflammatory cytokines (IL-1 β and IL-6), and tumor necrosis factor- α (TNF- α) were nullified in SBFO-treated THP-1 cells (human leukemia monocytic cell line). SBFO intervention reduced edema in Carrageenan-induced paw edema and mice psoriasis-like experimental models. The study in question claimed that SBFO could be used as an anti-inflammatory and anti-psoriatic candidate [27]. It is likely that topical application of SBO improved the AD-like lesions in the mouse model. Moreover, SBO suppressed the thymus- and activation-regulated chemokine and macrophage-derived chemokine via NF- κ b, Janus kinase 2/signal transducer and activators of transcription 1 (JAK2/STAT1), and p38 mitogen-activated protein kinase (p38-MAPK) pathways in HaCaT (spontaneously immortalized, human keratinocyte line) cells [13].

SB has been recognized as one of the active compounds used in skincare products. The effect of the combination of SB fruit extract, blueberry extract, and collagen on UV-induced skin aging was investigated using a mouse model [14]. The oral administration of the SB fruit blend for six weeks reduced wrinkle formation in the skin and maintained the normal moisture content by preventing transdermal water loss. The protective effect

of the SB fruit blend was associated with the expression of matrix metalloproteinase (MMP)-1 and MMP-9 and superoxide dismutase activity [14]. Gegotek et al. [15] described the influence of SB seed oil (SBSO) on UV-mediated alterations to lipid metabolism in skin (keratinocytes and fibroblasts) cells. The results showed that SBSO improved non-enzymatic antioxidant levels and inhibited UV-induced reactive oxygen species (ROS). The activity of nuclear erythroid 2-related factor (Nrf2) that was induced improved antioxidant enzyme activity. Phospholipid and free fatty acid levels were increased in SBSO-treated cells and decreased lipid peroxidation products and cannabinoid receptor expression. Changes in the expression of peroxisome proliferator-activated receptors (PPARs) were also noticed in SBSO-treated skin cells. The study suggested that SBSO could counteract UV-induced changes in lipid metabolism and redox balance, thereby protecting the skin against photo-damage [15].

Kaempferol, quercetin, isorhamnetin, and procyanidins are the major compounds in the hydroalcoholic extract of SB (HESB). HESB treatment significantly decreased melanin content and inhibited extracellular tyrosinase activity in B16F10 mouse melanoma cells. HESB suppressed the expression of tyrosinase (TYR) and tyrosinase-related protein 1 (TRP-1). The anti-melanogenesis property of HESB may be attributed to decreased TYR activity and expression of TRP-1 [28].

The purpose of this study was to develop SBO-NLCs for improved skin hydration. The particle size, PDI, ZP, and EE of the developed SBO-NLCs were characterized.

Particle size is the most essential parameter to be determined for the targeted delivery of active ingredients to specific sites [29]. Based on many previous studies, the use of various solid or liquid lipids or their combinations affects the particle size of developed NLCs. The selection of solid lipids was based on the particle size and specific target site. Both stearic fit and the solubility of the drug may affect the particle size of NLC formulations. The smallest particle size for the SBO-NLCs was 105.27 nm, which was predicted and experimentally proved. The results showed that the experimental design could predict the conditions to develop the optimum SBO-NLCs with respect to particle size (Table 2).

The PDI values provided information about the homogeneity of prepared NLCs [30]. Vegetable oil-loaded NLCs showed a PDI value of 0.281 to 0.382, and in the study in question it was claimed that the formulation was homogenous [31]. Curcumin-loaded NLC preparations with different oils (coconut, fish, black seed, and linseed oils) showed PDI values of 0.35 to 0.38 [32]. Argan oil-loaded NLCs and silybin-loaded NLCs showed PDI values of 0.21 ± 0.01 and 0.109 ± 0.008 , respectively [33,34]. Increased drug concentration increases PDI values; for example, lycopene-loaded NLCs exhibited increases in PDI values corresponding to drug concentrations [35]. In the present study, the actual PDI values were found to be between 0.16 and 0.37, which reflects the relatively homogeneous size of the SBO-NLCs (Table 2). As with PDI, ZP also reflects the homogeneity of NLC formulations. The ZP of lycopene-loaded NLCs was found to be between -73.8 and -74.6 mV, depending on the concentration of the drug [35]. The ZP of curcumin-loaded NLCs (-26.5 ± 1.8 to -32.0 ± 1.9 mV), argan oil-loaded NLCs (53.37 ± 0.92), and silybin-loaded NLCs (-19.5 ± 1.1 mV) were documented previously [32,34]. In the present study, actual ZPs between -15.63 (the optimum ZP) and -36.87 mV were observed for the SBO-NLCs (Table 2). We may conclude that the prepared SBO-NLC was a homogenized optimal NLC, according to particle size, PDI, and ZP values.

In the development of NLCs, EE percentage is an important factor to be considered. Compared to other drug delivery systems, NLCs have high EE percentages [29]. The drug solubility in the surfactant and lipid matrix used affect the EE. The protective surfactant layer of the NLC prevents drug leakage from the particles, thus helping to increase the EE percentage. The type of solid lipid used in NLCs greatly affects EE through the formation of different morphologies of NLCs and drug solubility in the lipid matrix. Approximately 99.98% of EE was documented with Precirol[®] ATO 5 as a solid lipid in the development of paclitaxel-loaded NLCs [36], while EE was observed to be between 82 and 98% when using

COMPRITOL® 888 ATO as lipid [29]. The EE percentage using glyceryl monostearate was between 48 and 87% [37,38]. Interestingly, in the present study, a 90.88% actual EE was observed using glyceryl monostearate as solid lipid (Table 2), which may be due to the combination of lipids, surfactant, and co-surfactant used in this study.

Thermal characterization of developed SBO-NLCs was performed using DSC. The method used for the characterization of biomolecules includes nucleic acid, carbohydrate protein, lipid, and thermal characterizations of NLCs [39]. The melting point of the SBO-NLCs was higher than 65 °C (Figure 5), which is one of the desirable properties of topical products [40]. The result showed a reduction in the melting peak of the SBO-NLCs (Table 5). This could be associated with the smaller size of the particles [34]. The results indicate a lower possibility of drug repulsion from the core matrix during storage due to the crystallinity deduction of the lipid matrix [41]. DSC suggested that the NLCs had less crystallinity, thereby reducing the amount of drug expulsion from the nanoparticle and resulting in a high EE percentage.

Increased trans-epidermal water is associated with disturbance to the stratum corneum and intercellular lipid loss, and skin dehydration causes a variety of skin problems. Thus, protecting the skin from dehydration is necessary and is one of the key characteristics of skin moisturizing agents. The high oil content may provide an occlusive barrier, preventing trans-epidermal water loss [42]. Loo et al. [43] stated that NLCs with high lipid contents improved skin hydration levels and prevented trans-epidermal water loss in human volunteers. The results of the current study suggested that the SBO-NLCs have a greater occultation effect, which presumably enhances skin hydration by preventing water loss through evaporation [25]. The occultation effect of the SBO-NLCs had a considerable range (Figure 7). Furthermore, the presence of lipids in SBO-NLCs could improve skin moisture content and prevent skin dryness.

The initial burst drug release was reported for tretinoin-loaded NLCs [40], lycopen-loaded NLCs [35], and silybin-loaded NLCs [34]. Some explanations for the rapid initial drug release have been provided in the literature. The crystalline structure of NLCs may be weaker, facilitating the sudden release of the drug. In another way, the drug release rate was high, due to the small size and high surface area and high diffusion coefficient of NLCs [34,35]. In addition, the *in vitro* release profile indicated the distribution of SBO in the lipid matrix [35]. The size, morphology, and surfactant of NLCs could affect the release profiles of active compounds [44,45]. SBO-NLCs could release the drug faster into the skin within 24 h, and the released drug level after 48 h was significantly higher than that for the free SBO (Figure 8). The results suggested that the SBO-NLCs have a satisfactory level of *in vitro* drug-releasing capability.

Previous studies also suggested that NLCs could deliver drugs effectively. For instance, a higher amount of drug permeation was observed for tenoxicam-loaded NLCs *in vitro* and *ex vivo* models. Comparatively, the nanoparticle permeation was higher than that of the pure drug [46]. Similarly, the *ex vivo* skin penetration of idebenone-loaded NLCs was significantly higher than the pure drug [47]. The drug permeation of charged NLC molecules was different and depended on the charge of the NLCs. Cationic NLCs could increase the permeability and deposition of a drug (tripterine) more effectively [48].

In vitro and *ex vivo* Franz cell systems are comparable to human skin. The SBO-NLCs delivered the drug into the inner skin significantly ($22.73 \pm 1.67 \mu\text{g}/\text{cm}^2$ of skin) (Figure 9b). The results of the present study showed the high drug permeation and deposition of SBO in the skin, and the developed NLCs were potent enough to transfer the SBO into the skin.

For the following factors, constraints were set to predict the optimum conditions for SBO-NLC development: wax (in the range of 2.5 to 7.5%), surfactant (in the range of 2.5 to 7.5%), PEG400 in surfactant (in the range of 10 to 30%), size (minimize), PDI (minimize), ZP (minimize), and EE (minimize). Accordingly, the experimental design for the optimum SBO-NLCs was predicted. It was predicted that the combination of 2, 5% wax, 7.5% surfactant, and 30% PEG in the surfactant could produce optimum SBO-NLCs

(size = 119.20 nm; PDI = 0.26; ZP = −21.45 mV; EE = 84.45%). The actual values were comparable to the predicted conditions.

5. Conclusions

Our study explains the influence of wax, surfactant, and PEG400 percentages in the surfactant on SBO-NLC development. There was a single condition needed to fulfill all the desirable features of SBO-NLCs that was not revealed in the study. However, the developed SBO-NLCs showed a desirable level of occlusion effect, drug release profile, and drug penetration. Thus, the SBO-NLCs could serve as a potential delivery system to prevent skin dehydration. Though the study results could help to construct an experimental model to produce the SBO-NLC, some key factors, such as the stability of the SBO-NLC, drug-loading capacity, and ex vivo and human experimental trials, are required to define the feasibility of the developed SBO-NLC. Thus, further studies are required to optimize the conditions in order to produce the optimum SBO-NLC.

Author Contributions: Conceptualization, C.C. and W.R.; methodology, C.C., D.J. and W.R.; validation, C.C. and W.R.; formal analysis, C.T., P.J., D.J. and K.C.; investigation, C.C. and C.T.; resources, D.J. and S.P.; data curation, C.T., P.J. and D.J.; writing—original draft preparation, C.C., B.S.S., C.T. and W.R.; writing—review and editing, C.C., B.S.S., C.T. and W.R.; visualization, C.T.; supervision, C.C. and W.R.; project administration, K.C. and S.P.; funding acquisition, C.C. All authors have read and agreed to the published version of the manuscript.

Funding: This project was supported by Fundamental fund 2022, Chiang Mai University, Chiang Mai, Thailand.

Institutional Review Board Statement: Not applicable.

Informed Consent Statement: Not applicable.

Data Availability Statement: The data presented in this study are available within the article.

Acknowledgments: The authors gratefully acknowledge the Faculty of Pharmacy and Chiang Mai University, Chiang Mai, Thailand, and the Faculty of Pharmaceutical Sciences, Ubon Ratchathani University, Thailand.

Conflicts of Interest: The authors declare no conflict of interest.

References

1. Rawlings, A.V.; Harding, C.R. Moisturization and skin barrier function. *Dermatol. Ther.* **2004**, *17*, 43–48. [[CrossRef](#)] [[PubMed](#)]
2. D’Orazio, J.; Jarrett, S.; Amaro-Ortiz, A.; Scott, T. UV radiation and the skin. *Int. J. Mol. Sci.* **2013**, *14*, 12222–12248. [[CrossRef](#)] [[PubMed](#)]
3. Purnamawati, S.; Indrastuti, N.; Danarti, R.; Saefudin, T. The Role of Moisturizers in Addressing Various Kinds of Dermatitis: A Review. *Clin. Med. Res.* **2017**, *15*, 75–87. [[CrossRef](#)] [[PubMed](#)]
4. Loden, M. The clinical benefit of moisturizers. *J. Eur. Acad. Dermatol. Venereol.* **2005**, *19*, 672–688. [[CrossRef](#)] [[PubMed](#)]
5. Pavlou, P.; Siamidi, A.; Varvaresou, A.; Vlachou, M. Skin Care Formulations and Lipid Carriers as Skin Moisturizing Agents. *Cosmetics* **2021**, *8*, 89. [[CrossRef](#)]
6. Müller, R.H.; Petersen, R.D.; Hommoss, A.; Pardeike, J. Nanostructured lipid carriers (NLC) in cosmetic dermal products. *Adv. Drug Deliv. Rev.* **2007**, *59*, 522–530. [[CrossRef](#)] [[PubMed](#)]
7. Pardeike, J.; Schwabe, K.; Müller, R.H. Influence of nanostructured lipid carriers (NLC) on the physical properties of the Cutanova Nanorepair Q10 cream and the in vivo skin hydration effect. *Int. J. Pharm.* **2010**, *396*, 166–173. [[CrossRef](#)] [[PubMed](#)]
8. Olas, B. The beneficial health aspects of sea buckthorn (*Elaeagnus rhamnoides* (L.) A. Nelson) oil. *J. Ethnopharmacol.* **2018**, *213*, 183–190. [[CrossRef](#)] [[PubMed](#)]
9. Ren, R.; Li, N.; Su, C.; Wang, Y.; Zhao, X.; Yang, L.; Li, Y.; Zhang, B.; Chen, J.; Ma, X. The bioactive components as well as the nutritional and health effects of sea buckthorn. *RSC Adv.* **2020**, *10*, 44654–44671. [[CrossRef](#)] [[PubMed](#)]
10. Guo, R.; Guo, X.; Li, T.; Fu, X.; Liu, R.H. Comparative assessment of phytochemical profiles, antioxidant and antiproliferative activities of Sea buckthorn (*Hippophae rhamnoides* L.) berries. *Food Chem.* **2017**, *221*, 997–1003. [[CrossRef](#)] [[PubMed](#)]
11. Hou, D.; Wang, D.; Ma, X.; Chen, W.; Guo, S.; Guan, H. Effects of total flavonoids of sea buckthorn (*Hippophae rhamnoides* L.) on cytotoxicity of NK92-MI cells. *Int. J. Immunopathol. Pharmacol.* **2017**, *30*, 353–361. [[CrossRef](#)] [[PubMed](#)]
12. Shi, L.; Zheng, L.; Zhao, C.; Jin, Q.; Wang, X. Chemical composition and antioxidant capacity of extracts from the whole berry, pulp and seed of *Hippophae rhamnoides* ssp. *yunnanensis*. *Nat. Prod. Res.* **2019**, *33*, 3596–3600. [[CrossRef](#)]

13. Hou, D.D.; Di, Z.H.; Qi, R.Q.; Wang, H.X.; Zheng, S.; Hong, Y.X.; Guo, H.; Chen, H.D.; Gao, X.H. Sea Buckthorn (*Hippophae rhamnoides* L.) Oil Improves Atopic Dermatitis-Like Skin Lesions via Inhibition of NF- κ B and STAT1 Activation. *Skin Pharmacol. Physiol.* **2017**, *30*, 268–276. [[CrossRef](#)] [[PubMed](#)]
14. Hwang, I.S.; Kim, J.E.; Choi, S.I.; Lee, H.R.; Lee, Y.J.; Jang, M.J.; Son, H.J.; Lee, H.S.; Oh, C.H.; Kim, B.H.; et al. UV radiation-induced skin aging in hairless mice is effectively prevented by oral intake of sea buckthorn (*Hippophae rhamnoides* L.) fruit blend for 6 weeks through MMP suppression and increase of SOD activity. *Int. J. Mol. Med.* **2012**, *30*, 392–400. [[CrossRef](#)]
15. Gegotek, A.; Jastrzab, A.; Jarocka-Karpowicz, I.; Muszyńska, M.; Skrzydlewska, E. The Effect of Sea Buckthorn (*Hippophae rhamnoides* L.) Seed Oil on UV-Induced Changes in Lipid Metabolism of Human Skin Cells. *Antioxidants* **2018**, *7*, 110. [[CrossRef](#)]
16. Woraharn, S.; Lailerd, N.; Sivamaruthi, B.S.; Wangcharoen, W.; Peerajan, S.; Sirisattha, S.; Chaiyasut, C. Development of fermented *Hericium erinaceus* juice with high content of L-glutamine and L-glutamic acid. *Int. J. Food Sci. Technol.* **2015**, *50*, 2104–2112. [[CrossRef](#)]
17. Chaiyasut, C.; Pengkumsri, N.; Sirilun, S.; Peerajan, S.; Khongtan, S.; Sivamaruthi, B.S. Assessment of changes in the content of anthocyanins, phenolic acids, and antioxidant property of *Saccharomyces cerevisiae* mediated fermented black rice bran. *AMB Express* **2017**, *7*, 114. [[CrossRef](#)]
18. Bezerra, M.A.; Santelli, R.E.; Oliveira, E.P.; Villar, L.S.; Escalera, L.A. Response surface methodology (RSM) as a tool for optimization in analytical chemistry. *Talanta* **2008**, *76*, 965–977. [[CrossRef](#)]
19. Atul Anand, P.; Praveen Digambar Chaudhari, P.D. Development and Evaluation of Nanostructured Lipid Carrier (NLC) Based Topical Delivery of an Anti-Inflammatory Drug. *J. Pharm. Res.* **2013**, *7*, 677–685.
20. Moghddam, S.M.; Ahad, A.; Aqil, M.; Imam, S.S.; Sultana, Y. Optimization of nanostructured lipid carriers for topical delivery of nimesulide using Box-Behnken design approach. *Artif. Cells Nanomed. Biotechnol.* **2017**, *45*, 617–624. [[CrossRef](#)]
21. Trakoolthong, P.; Ditthawuttikul, N.; Sivamaruthi, B.S.; Sirilun, S.; Rungseevijitprapa, W.; Peerajan, S.; Chaiyasut, C. Antioxidant and 5 α -Reductase Inhibitory Activity of *Momordica charantia* Extract, and Development and Characterization of Microemulsion. *Appl. Sci.* **2022**, *12*, 4410. [[CrossRef](#)]
22. Cirri, M.; Maestrini, L.; Maestrelli, F.; Mennini, N.; Mura, P.; Ghelardini, C.; Di Cesare Mannelli, L. Design, characterization and in vivo evaluation of nanostructured lipid carriers (NLC) as a new drug delivery system for hydrochlorothiazide oral administration in pediatric therapy. *Drug Deliv.* **2018**, *25*, 1910–1921. [[CrossRef](#)] [[PubMed](#)]
23. Dolatabadi, S.; Karimi, M.; Nasirizadeh, S.; Hatamipour, M.; Shiva Golmohammadzadeh, S.; Jaafari, M.R. Preparation, characterization and in vivo pharmacokinetic evaluation of curcuminoids-loaded solid lipid nanoparticles (SLNs) and nanostructured lipid carriers (NLCs). *J. Drug Deliv. Sci. Technol.* **2021**, *62*, 102352. [[CrossRef](#)]
24. Anantaworasakul, P.; Chaiyana, W.; Michniak-Kohn, B.B.; Rungseevijitprapa, W.; Ampasavate, C. Enhanced Transdermal Delivery of Concentrated Capsaicin from Chili Extract-Loaded Lipid Nanoparticles with Reduced Skin Irritation. *Pharmaceutics* **2020**, *12*, 463. [[CrossRef](#)]
25. Krambeck, K.; Silva, V.; Silva, R.; Fernandes, C.; Cagide, F.; Borges, F.; Santos, D.; Otero-Espinar, F.; Lobo, J.M.S.; Amaral, M.H. Design and characterization of Nanostructured lipid carriers (NLC) and Nanostructured lipid carrier-based hydrogels containing *Passiflora edulis* seeds oil. *Int. J. Pharm.* **2021**, *600*, 120444. [[CrossRef](#)]
26. Gaba, B.; Fazil, M.; Khan, S.; Ali, A.; Baboota, S.; Ali, J. Nanostructured lipid carrier system for topical delivery of terbinafine hydrochloride. *Bull. Fac. Pharm. Cairo Univ.* **2015**, *53*, 147–159. [[CrossRef](#)]
27. Balkrishna, A.; Sakat, S.S.; Joshi, K.; Joshi, K.; Sharma, V.; Ranjan, R.; Bhattacharya, K.; Varshney, A. Cytokines Driven Anti-Inflammatory and Anti-Psoriasis Like Efficacies of Nutraceutical Sea Buckthorn (*Hippophae rhamnoides*) Oil. *Front. Pharmacol.* **2019**, *10*, 1186. [[CrossRef](#)]
28. Zhang, J.; Wang, C.; Wang, C.; Sun, B.; Qi, C. Understanding the role of extracts from sea buckthorn seed residues in anti-melanogenesis properties on B16F10 melanoma cells. *Food Funct.* **2018**, *9*, 5402–5416. [[CrossRef](#)]
29. Apostolou, M.; Assi, A.; Fatokun, A.A.; Khan, I. The Effects of Solid and Liquid Lipids on the Physicochemical Properties of Nanostructured Lipid Carriers. *J. Pharm. Sci.* **2021**, *110*, 2859–2872. [[CrossRef](#)]
30. Pinto, M.F.; Moura, C.C.; Nunes, C.; Segundo, M.A.; Lima, S.A.C.; Reis, S. A new topical formulation for psoriasis: Development of methotrexate-loaded nanostructured lipid carriers. *Int. J. Pharm.* **2014**, *477*, 519–526. [[CrossRef](#)]
31. Pinto, F.; de Barros, D.P.C.; Fonseca, L.P. Design of multifunctional nanostructured lipid carriers enriched with α -tocopherol using vegetable oils. *Ind. Crops Prod.* **2018**, *118*, 149–159. [[CrossRef](#)]
32. Saedi, A.; Rostamizadeh, K.; Parsad, M.; Dalalia, N.; Ahmadi, N. Preparation and characterization of nanostructured lipid carriers as drug delivery system: Influence of liquid lipid types on loading and cytotoxicity. *Chem. Phys. Lipids* **2018**, *216*, 65–72. [[CrossRef](#)] [[PubMed](#)]
33. Tichota, D.M.; Silva, A.C.; Sousa Lobo, J.M.; Amaral, M.H. Design, characterization, and clinical evaluation of argan oil nanostructured lipid carriers to improve skin hydration. *Int. J. Nanomed.* **2014**, *9*, 3855–3864.
34. Jia, L.J.; Zhang, D.R.; Li, Z.Y.; Feng, F.F.; Wang, Y.C.; Dai, W.T.; Duan, C.X.; Zhang, Q. Preparation and characterization of silybin-loaded nanostructured lipid carriers. *Drug Deliv.* **2010**, *17*, 11–18. [[CrossRef](#)] [[PubMed](#)]
35. Okonogi, S.; Riangjanapatee, P. Physicochemical characterization of lycopene-loaded nanostructured lipid carrier formulations for topical administration. *Int. J. Pharm.* **2015**, *478*, 726–735. [[CrossRef](#)]
36. Bang, K.H.; Na, Y.G.; Huh, H.W. The delivery strategy of paclitaxel nanostructured lipid carrier coated with platelet membrane. *Cancers* **2019**, *11*, 807. [[CrossRef](#)] [[PubMed](#)]

37. Zhang, X.; Gan, Y.; Gan, L.; Nie, S.; Pan, W. PEGylated nanostructured lipid carriers loaded with 10-hydroxycamptothecin: An efficient carrier with enhanced antitumour effects against lung cancer. *J. Pharm. Pharmacol.* **2010**, *60*, 1077–1087. [[CrossRef](#)] [[PubMed](#)]
38. Shao, Z.; Shao, J.; Tan, B. Targeted lung cancer therapy: Preparation and optimization of transferrin-decorated nanostructured lipid carriers as novel nanomedicine for co-delivery of anticancer drugs and DNA. *Int. J. Nanomed.* **2015**, *10*, 1223–1233. [[CrossRef](#)] [[PubMed](#)]
39. Gill, P.; Moghadam, T.T.; Ranjbar, B. Differential Scanning Calorimetry Techniques: Applications in Biology and Nanoscience. *J. Biomol. Tech.* **2010**, *21*, 167–193.
40. Ghate, V.K.; Lewis, S.A.; Prabhakara Prabhu, P.; Dubey, A.; Patel, N. Nanostructured lipid carriers for the topical delivery of tretinoin. *Eur. J. Pharm. Biopharm.* **2016**, *108*, 253–261. [[CrossRef](#)] [[PubMed](#)]
41. Chauhan, I.; Yasir, M.; Verma, M.; Singh, A.P. Nanostructured Lipid Carriers: A Groundbreaking Approach for Transdermal Drug Delivery. *Adv. Pharm. Bull.* **2020**, *10*, 150–165. [[CrossRef](#)] [[PubMed](#)]
42. Choi, W.S.; Cho, H.I.; Lee, H.Y.; Lee, S.H.; Choi, Y.W. Enhanced Occlusiveness of Nanostructured Lipid Carrier (NLC)-based Carbogel as a Skin Moisturizing Vehicle. *J. Pharm. Investig.* **2010**, *40*, 373–378.
43. Loo, C.h.; Basri, M.; Ismail, R.; Lau, H.; Tejo, B.; Kanthimathi, M.; Hassan, H.; Choo, Y. Effect of compositions in nanostructured lipid carriers (NLC) on skin hydration and occlusion. *Int. J. Nanomed.* **2013**, *8*, 13–22. [[CrossRef](#)] [[PubMed](#)]
44. Souto, E.B.; Wissing, S.A.; Barbosa, C.M.; Muller, R.H. Development of a controlled release formulation based on SLN and NLC for topical clotrimazole delivery. *Int. J. Pharm.* **2004**, *278*, 71–77. [[CrossRef](#)] [[PubMed](#)]
45. Luo, Y.; Chen, D.W.; Ren, L.X.; Zhao, X.L.; Qin, J. Solid lipid nanoparticles for enhancing vinpocetine's oral bioavailability. *J. Control. Release* **2006**, *114*, 53–59. [[CrossRef](#)] [[PubMed](#)]
46. Bawazeer, S.; El-Telbany, D.F.A.; Al-Sawahli, M.M.; Zayed, G.; Keed, A.A.A.; Abdelaziz, A.E.; Abdel-Naby, D.H. Effect of nanostructured lipid carriers on transdermal delivery of tenoxicam in irradiated rats. *Drug Deliv.* **2020**, *27*, 1218–1230. [[CrossRef](#)] [[PubMed](#)]
47. Li, B.; Ge, Z. Nanostructured Lipid Carriers Improve Skin Permeation and Chemical Stability of Idebenone. *AAPS PharmSciTech.* **2012**, *13*, 276–283. [[CrossRef](#)] [[PubMed](#)]
48. Chen, Y.; Zhou, L.; Yuan, L.; Zhang, Z.H.; Liu, X.; Wu, Q. Formulation, characterization, and evaluation of in vitro skin permeation and *in vivo* pharmacodynamics of surface-charged tripterine-loaded nanostructured lipid carriers. *Int. J. Nanomed.* **2012**, *7*, 3023–3032.